Materials Science & Engineering C 105 (2019) 110093

Contents lists available at ScienceDirect

Materials Science & Engineering C

journal homepage: www.elsevier.com/locate/msec

Potential for combined delivery of riboflavin and all-trans retinoic acid, from silk fibroin for corneal bioengineering

Promita Bhattacharjee[a,b], Julia Fernández-Pérez[a,b], Mark Ahearne[a,b,*]

[a] Trinity Centre for Biomedical Engineering, Trinity Biomedical Sciences Institute, Trinity College Dublin, University of Dublin, Dublin, Ireland
[b] Department of Mechanical and Manufacturing Engineering, School of Engineering, Trinity College Dublin, University of Dublin, Dublin, Ireland

ARTICLE INFO

Keywords:
Retinoic acid
Cornea
Fibroin
Regeneration
Riboflavin
Stroma

ABSTRACT

Millions of people worldwide suffer from vision impairing conditions resulting from corneal injury or disease. Silk fibroin (SF) is an emerging biopolymer that has been used for several applications including the fabrication of bioengineered corneas and ocular prostheses. To improve the cell response to SF, riboflavin (RF) and all-trans retinoic acid (RA) were coupled onto SF matrices. RF is a photo-initiator that has previously been combined with ultraviolet light to crosslink corneal collagen while RA has been used to regulate the phenotype of corneal stromal cells and their extracellular matrix deposition. Different concentrations of RF and RA were respectively photo-crosslinked and covalently bound through carbodiimide coupling onto 2% SF matrices. The effect of incorporating these molecules on the physical, chemical and mechanical properties of the matrices was evaluated. The biological response of human corneal stromal cells to the matrices was examined using cellular adhesion assays, proliferation assays, cytoskeleton staining, gene expression analysis and immunocytochemical staining. RF and RA both led to changes in the surface nanostructure and hydrophilicity while just RF increased the material stiffness. Cells cultured on the matrices containing both biomolecules displayed improved cellular proliferation, increased GAG deposition and increased expression of keratocyte genes that are normally associated with healthy corneal stromal tissue. These *in vitro* studies serve as a starting point for the optimization of loading bioactive molecules on SF based matrices for formulating clinically relevant ocular implants.

1. Introduction

Damage to the cornea, from injury or disease, can compromise visual acuity and may lead to blindness. There are an estimated 4.9 million cases of bilateral corneal blindness and 23 million cases of unilateral corneal blindness worldwide [1]. A cornea transplant is often the only suitable treatment to regain vision however the success of these transplants can be affected by many factors including wound healing, mismatch of donor and recipient tissue size, curvature and thickness and astigmatism due to sutures [2]. The limited availability and accessibility of transplantable donated corneas is another issue that needs to be considered since it limits the number of possible procedures [3]. One solution to overcoming these issues is to develop bioengineered corneal tissue as an alternative to allogenic donor corneas for transplantation.

When trying to engineer corneal tissue it is important to choose a scaffold material that has suitable physical and optical characteristics while also promoting a functional cell phenotype. Through decades of sustained investigations that revealed attractive properties like biocompatibility, cytocompatibility, biodegradability, mechanical strength and an ability to stabilize labile compounds, silk fibroin (SF) has established itself as a promising biopolymer for many medical applications [4–6]. In addition, since SF is nearly fully transparent to visible light, it can also be used for fabricating ocular constructs [7–11]. Such a combination of properties appears to make silk an attractive material for the fabrication of corneal scaffolds.

While SF has superior mechanical properties than many other natural biopolymers, these can be further enhanced by crosslinking. Although ruthenium is known to be capable of photo-crosslinking silk [12], the possible toxicity of ruthenium [13] means options for a nontoxic photo initiator are being examined for use *in vivo*. To this end, riboflavin (RF) has been explored as a crosslinking agent since it is naturally found in tissues and it can be used as a photoinitiator by exposing it to visible and ultra-violet light of wavelengths between 330 and 470 nm (peak absorbance 350–450 nm and fluorescence emission peak at 533 nm) [14]. It has previously been used to crosslink polymers

* Corresponding author at: Trinity Centre for Biomedical Engineering, Trinity Biomedical Sciences Institute, Trinity College Dublin, University of Dublin, Dublin 2, Ireland.
E-mail address: ahearnm@tcd.ie (M. Ahearne).

https://doi.org/10.1016/j.msec.2019.110093
Received 10 October 2018; Received in revised form 8 August 2019; Accepted 15 August 2019
Available online 15 August 2019

such as collagen [15–17], polysaccharides [18] and poly(ethylene glycol) [19].

In addition to providing a construct for cells to attach, ideally scaffolds should contain molecules that positively influence cell behavior. For example, all-trans retinoic acid (RA) is essential to cellular differentiation and homeostasis, vertebrate development, and ocular health [20]. RA is a metabolic derivative Vitamin A and plays a crucial role in development and signaling processes in the eye [21]. It also has been shown to support a corneal stromal keratocyte phenotype under serum free conditions [22,23].

RF and RA have been used individually in studies investigating corneal regeneration. A combined delivery of both molecules has not previously been explored and specifically by using a SF matrix. Indeed, while photo-crosslinked SF-RF matrices have showed promise as an ocular prostheses [7], loading SF with RA has not previously been explored for corneal regeneration. In the current work, both bioactive molecules, at different loading concentrations, were covalently coupled onto SF matrices. Loading concentrations were optimized based on the results of mechanical testing and the biocompatibility of human corneal stromal cells. SF matrices with the optimal loading concentrations were then subjected to detailed *in vitro* studies. Since RF and RA are both expressed as part of corneal stroma repair, it was hypothesized that their dual delivery within a scaffold will result in enhanced stroma regeneration.

2. Materials and methods

Unless otherwise specified, chemicals and reagents were purchased from Sigma-Aldrich.

2.1. Isolation of silk fibroin from Bombyx mori cocoon

Silk fibroin (SF) from *Bombyx mori* (Bm) cocoons (Treenway silks, USA) was extracted using a standard protocol [7]. In summary, the cocoons were boiled in 0.02 M sodium carbonate solution to extract SF, separating out serecin – the glue like component that holds cocoons together. Extracted SF was dissolved in 9.3 M lithium bromide at 60 °C, allowing 4 h for complete dissolution. This solution was dialyzed, over 72 h against deionized water. Dialysis removed the lithium bromide. The SF concentration was adjusted, using 10% (w/v) Polyethylene glycol (PEG, 10,000 MW) solution, to 2% (wt/wt) and this concentration was used throughout this study.

2.2. Fabrication of riboflavin (RF) and all-trans RA crosslinked silk fibroin matrices

RF at concentrations of 0.2 mM, 2.5 mM, 10 mM and 20 mM were used to crosslink 2% SF. Crosslinking was triggered using UVA light in an otherwise dark room. This crosslinking process has been represented using Fig. 1(a). Each RF molecule creates a linkage between two molecules of SF repeat units. To perform crosslinking, a parallel plate arrangement was used. A quartz plate was positioned on the top and a stainless-steel plate formed the base. Temperature was maintained at 37 °C for 60 min. To provide the required illumination upon the SF matrices, a light source with a peak emission wavelength of 365 nm was used. After air-drying, crosslinked SF matrices were treated with absolute ethanol for 5 min and 70% ethanol for 20 min to form a β-sheet structure.

All-trans RA concentrations of 0.5 μM, 2.5 μM, 5 μM and10 μM were covalently coupled onto β-sheet formed silk fibroin matrix using carbodiimide coupling reaction over 8 h. To conjugate all-trans RA and SF via a stable amide bond, N-(3-Dimethylaminopropyl)-N′-ethylcarbodiimide hydrochloride (EDC)/N-Hydroxysuccinimide (NHS) was used. The mechanism has been represented in Fig. 1(b).

The SF matrices were fabricated by solution casting. SF solution was put onto a horizontal dish and following the solution's evaporation, the matrix was collected. Matrix thickness was controlled by altering volume of casting solution.

2.3. Mechanical characterization

Following the ASTM 638-5 standard, matrices undergoing mechanical testing were cut into dumbbell shaped samples (50 mm long, 10 mm wide) prior to tensile testing (UTM; Instron Electroplus, E1000). This test used a 10 kN load-cell, 3 mm/min extension rate and was conducted at 25 °C temperature and 50% relative humidity. The samples for tensile testing had been hydrated using PBS. Young's modulus of the matrices was calculated from the linear region of stress-strain curves < 3% strain.

2.4. Cell isolation and culture

Human corneal stromal cells were isolated from donor tissue as previously described [24] in accordance with the Declaration of Helsinki. Briefly, the epithelium and endothelium of the corneas were physically removed and the remaining stromal tissue was cut into small pieces and placed onto a culture plate. The tissue was then submerged in culture media consisting of Dulbecco's Low Glucose Modified Eagles Medium (DMEM) (Hyclone; Thermo Fisher Scientific) and supplemented with 10% fetal calf serum (Hyclone) and 1% penicillin/streptomycin. Once cells had migrated out from the stromal tissue and reached 80–90% confluency, they were trypsinized, centrifuged and suspended in the medium to be counted using a hemocytometer. The cells were then cultured in standard culture flasks in a controlled, humidified environment of 5% CO_2, at 37 °C. Cells at passage 3 were used in this study.

The silk matrices (1 × 1 cm^2) were sterilized by washing with 70% ethanol followed by a 20 min exposure to UV. They were then washed thrice using sterile PBS (pH 7.4) over 20 min and soaked in culture medium for 4 h to ensure that the matrices would provide a conducive environment to the seeded cells. A couple of hours before cell seeding, the matrices were partly dried to allow better cell penetration. Onto each matrix, 10 μl of cell suspension in media, that contained 1000 cells, was seeded drop-by-drop. For 1 h after cell-seeding, these matrices were kept in at 37 °C and 5% CO_2, in a humidified environment to bolster cell adhesion. Matrices were maintained using a serum free media consisting of DMEM/F12 (Hyclone; Thermo Fisher Scientific) supplemented with 1% penicillin/streptomycin, 100 μg/ml L-ascorbic acid and 1 μl/ml Insulin-Transferrin-Selenium (100×, Gibco) medium for up to 21 days, with media being replaced every alternate day.

2.5. Cell adhesion, metabolic activity and toxicity assays

Cell adhesion onto matrices was calculated based on the concentration of unattached cells left in the culture media 1, 3 and 5 h post cell seeding. Without disturbing the cell laden matrices, culture media was flushed carefully onto the culture plate. This detached any cells that might have been attached to the culture plate. Ten microliters of this cell suspension was placed into a chamber of the hemocytometer to calculate the concentration of unattached cells. The number of cells that adhered to the matrices was calculated by subtracting the density of unattached cells from the cell seeding density [25].

Over 21 days of cell culture, cell metabolic activity was assessed at several time points using a PrestoBlue assay (Molecular Probes; Invitrogen, Carlsbad, CA), following the manufacturer's protocols. Prestoblue™ is a blue non-fluorescent, cell permeable compound (resazurin-based solution), that is reduced by living cells into a fluorescent compound (resorufin). Briefly, 100 μl PrestoBlue™ was pipetted per well. After 1 h incubation in the dark, 200 μL dye-containing medium from each well was placed into 96-well plate in triplicate and the fluorescence intensity was measured using a fluorescence reader at an excitation and emission wavelengths of 570 nm and 600 nm

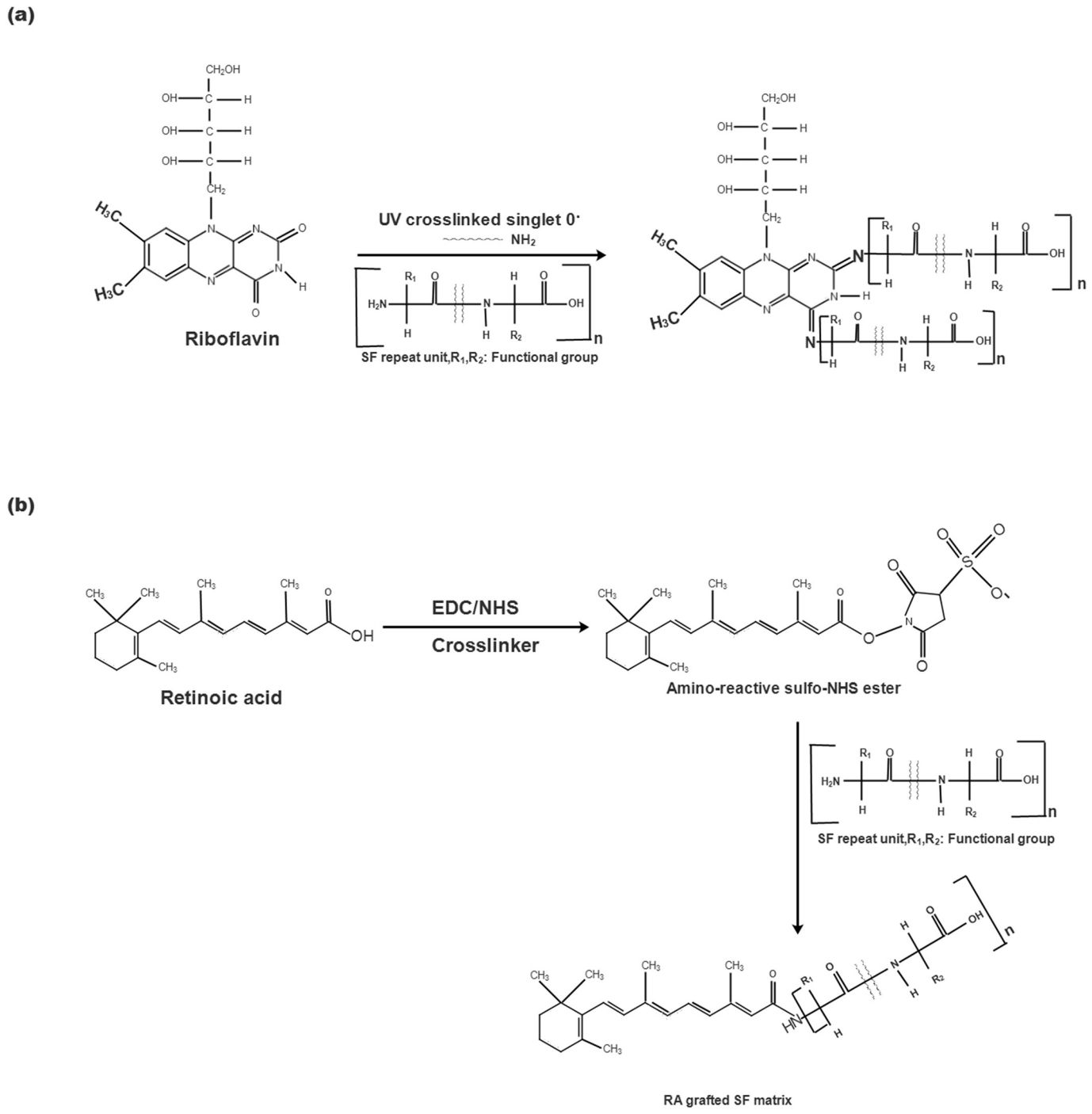

Fig. 1. (a) The schematic representation of UV crosslinked mechanism of RF and SF. (b) The schematic representation of RA incorporation on SF matrix by carbodiimide coupling reaction.

respectively.

A MTT assay was performed at different time points over the culture period to evaluate the toxicity of the fabricated matrices on cells. The cell seeded matrices were incubated within MTT solution for 2 h [5 mg/ml stock solution diluted in PBS (pH 7.4) at a 1:10 ratio]. This resulted in the formation of the formazan crystals, which were dissolved in dimethyl sulfoxide and measured using spectrophotometry at wavelength 595 nm (in accordance with the manufacturer's protocol).

2.6. Physical, chemical and thermal characterization on selected silk fibroin matrices

Following mechanical characterization and preliminary cell culture studies, 2.5 mM RF and 10 μM RA crosslinked SF matrices were found to have the most promising results for cell growth and proliferation. Hence, 2.5 mM RF and 10 μM RA were chosen for the combined loading study. Both bioactive molecules were covalently coupled with SF matrix, RF via photocrosslinking and RA via carbodiimide coupling reaction. The matrices were subsequently subjected to detailed biophysical, mechanical and biocompatibility studies.

Matrix surface morphology and chemical microanalysis (EDS) were

conducted using a Helium Ion Scanning Electron Microscope (Zeiss). Atomic force microscopy (AFM; Agilent Technologies, USA, Model 5100,) was used to investigate the matrix surface topography and roughness, over $2 \times 2\,\mu m^2$ area. AFM images were analyzed by Pico Image Basic Software (Agilent Technologies) to provide surface roughness, expressed as a surface root mean square (RMS) roughness (Rq).

Attenuated total reflectance-Fourier transform infrared (ATR-FTIR, Nexus-870, Thermo Nicolet Corporation, USA) was performed to analyze the chemical composition of the matrices. The spectra were recorded over a wave number range of 2500–500 cm^{-1} under ambient conditions. X-ray diffraction (XRD) patterns of fabricated matrices were recorded on an X-ray diffractometer (D8 discovery, Bruker) with CuKα radiation. The scanning range was from 10° to 70° in 2θ, at a speed of 2° per min. Differential scanning calorimetry (DSC; NETZSCH DSC 200PC), at a scanning rate of 10 °C/min, between 40 °C and 350 °C, was used to analyze the thermal property of the matrices. During the scan, liquid nitrogen flow at a rate of 50 ml/min was used for cooling.

After soaking in PBS at 37 °C for 7 days, matrices were tested for light transmission. The matrices were placed in a 12-well plate with PBS. PBS only was used as a blank control. The light transmittance was evaluated for wavelengths between 400 nm and 750 nm, using a microplate reader (Synergy HTX, purchased from BioTek). Refractive index was measured using a refractometer (Optilab). For each sample, an average of three measurements under each wavelength measured was taken.

Advancing and receding contact angles of fabricated matrices with respect to water were determined using an optical contact angle measuring system, a goniometer (Data Physics Instruments, Filderstadt, Germany). This assessed the hydrophilicity of these matrices.

2.7. In vitro RF and RA release from crosslinked matrices

The SF matrices crosslinked using RF were incubated for 28 days in deionized water at 37 °C to determine their release kinetics. RF released into the deionized water was estimated using absorbance measured at 270 nm [26]. The standard curve was made using deionized water.

High-performance liquid chromatography (HPLC) (Agilent Technology, Santa Clara, CA) was used to assay the all-trans RA released from SF matrices. For chromatography, the mobile phase consisted of 84.5%:15.0%:0.5% (v/v/v) acetonitrile: water: glacial acetic acid mixture. The UV detector was set at 353 nm to detect RA. At ambient temperature, a flow rate of 1.5 ml/min for injection volume 20 μl was used. Quantitative assessment of RA released from RA coupled SF matrices, at different time points over the 28 days, was obtained on the basis of a calibration curve ($r^2 = 0.99$, over RA concentrations of 0.02–100 μg/ml).

2.8. Enzymatic degradation

After incubation at 37 °C in 2 ml solution of 1.0 mg/ml Protease XIV (from Streptomyces griseus, Sigma) in PBS, SF matrices and SF matrices loaded with the two bio-molecules ($1 \times 1\,cm^2$, n = 5) were collected at 1, 7, 14 and 21 days. These matrices were weighed to calculate enzymatic degradation. During the incubation, the enzyme solution was replaced every other day. For control samples, incubation in PBS was carried out.

2.9. In vitro biocompatibility

Cells were seeded onto matrices using a 15 μl cell suspension that contained 3×10^4 cells. A live/dead assay was performed after 7 days of culture. The assay utilized dyes from Molecular Probes, USA and manufacturer's protocol was followed. Live cells were stained by calcein (green coloration; excitation: 488 nm) and dead cells by ethidiumhomodimer (red coloration; excitation: 543 nm). The stained matrices were examined using confocal microscopy (Leica SP8, Leica). Metabolic activity (MTT assay) was evaluated at different cell concentrations (1.5×10^4 cells/cm^2, 4.5×10^4 cells/cm^2 and 6×10^4 cells/cm^2).

2.10. Immunofluorescent staining

After 14 days of cell culture, cell laden matrices were fixed using 4% paraformaldehyde for 15 minute incubation at room temperature (RT). Matrices were permeabilized using 0.1% Triton X-100 solution in bovine serum albumin (BSA). They were then blocked using 1% BSA for 1 h. Actin filaments were stained with using phalloidin-TRITC and nuclei were stained using 4′,6-diamidino-2-phenylindole (DAPI). For immunocytochemical staining, fixed and permeabilized matrices were incubated for 30 min, in a blocking buffer of 2% (wt/vol) solution of BSA in PBS. These matrices were then incubated at 4 °C in anti-keratocan 1:50 (sc-66,941; Santa Cruz, Heidelberg, Germany), anti-ALDH3A1 1:50 (ab76976; Abcam, Cambridge, United Kingdom) or anti-α-smooth muscle actin (αSMA) 1:50 (ab7817; Abcam), for 18 h. This incubation was followed by matrices being rinsed with PBS and incubated at room temperature for an hour in fluorescently labelled antibodies in a dark room. Donkey anti-rabbit AlexaFluor 488 (ab150073; Abcam) was used to detect keratocan and ALDH3A1 and goat anti-mouse biotin was used for αSMA followed by ExtrAvidin-FITC (B7151 and E2761). Mouse monoclonal anti-vinculin antibody (Abcam) (1:400 dilution), identified by AlexaFluor 488 conjugated rabbit anti-mouse IgG (Abcam) (1:200 dilution), was used to stain vinculin. Cells were rinsed in PBS and incubated with 1 mg/mL DAPI in 1:500 dilution for nuclear staining. A 1.0% BSA was used for dilution of all antibodies. The Leica SP8 confocal microscope was used for imaging, followed by image post-processing using LAS X Advanced software. Cell shape was also quantified (cellular aspect ratio: length/width, n = 15) using post-processing software (Image J, NIH). Total cell density was quantified by drawing a box (5 cm × 5 cm) and counting the number of cells in this specific region (analyzed 10-unit area of 5 different images) of each fabricated matrix.

2.11. Gene expression by real-time Real Time-PCR

To quantify relative gene expression, at day 14 and 28, real-time reverse transcription PCR was used as previously described [27]. The following primers (Applied Biosystems, Biosciences, Dublin, Ireland) were examined: αSMA (Hs00426835_g1), ALDH3A1 (Hs00964880_m1), collagen type III (COL3A1; Hs00943809_m1), collagen type I (COL1A1; Hs00164004_m1), collagen type V (COL5A1; Hs00609133_m1), decorin (DCN; Hs00754870_s1), glyceraldehyde-3-phosphate dehydrogenase (GAPDH; Hs02758991_g1), keratocan (KERA; Hs00559942_m1), and lumican (LUM; Hs00929860_m1). For reference, gene expressions were normalized against GAPDH, based on the ΔΔCt method. The gene expression values thus calculated were expressed as an exponential form of $2^{-\Delta\Delta Ct}$.

2.12. Biochemical assays

Biochemical analysis of sulfated glycosaminoglycans (sGAG) and DNA was performed as previously described after 14 and 28 days in culture [28]. Using a digestion solution (125 μg/ml papain, 5 mM L-cysteine, 100 mM Na_2HPO_4, 5 mM EDTA, pH 6.8) cells on the matrices were macerated at 60 °C for 16 h. To quantify sGAG a dimethylmethylene blue (DMMB) binding assay (Blyscan; Biocolor Ltd., Antrim, UK) was used. Each sample was mixed with the DMMB solution and the absorbance was measured at 590 nm wavelength. Total sGAG of each sample was extrapolated using a standard plot of bovine chondroitin sulfate. To normalize data to DNA, a Bisbenzimide Hoechst 33258 DNA assay was used.

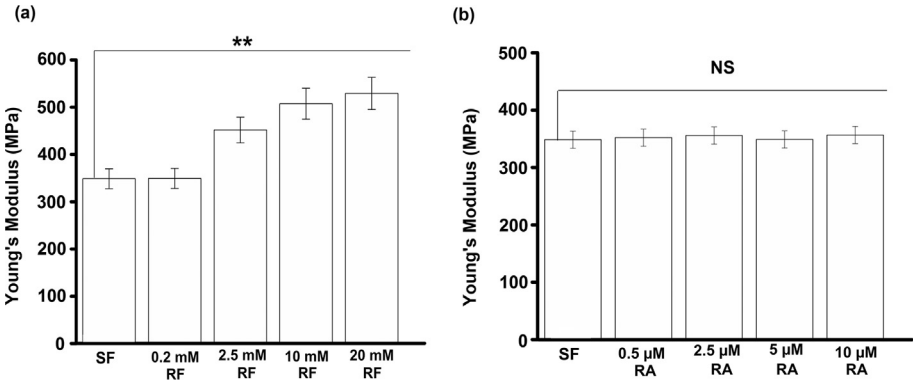

Fig. 2. Young's modulus of (a) different concentration of RF crosslinked and (b) different concentration of RA loaded SF matrices. A significant difference (**$p < 0.01$) in Young's modulus (MPa) observed with increased concentration of RF crosslinked SF matrices whereas no significant increment was not recorded for different concentration of RA grafted SF matrices.

2.13. Statistical analysis

To compare the results obtained for different matrix compositions, one-way ANOVA was used, followed by Tukey's post-hoc HSD test. Significant differences are represented as ***$p < 0.001$; **$p < 0.01$; *$p < 0.05$. Data presented uses the format of mean ± standard deviation (SD). Sample size, unless otherwise stated, remained 3.

3. Results and discussion

3.1. Influence of RF and RA loading concentration on the mechanical properties and biocompatibility of SF

The effect of RF and RA on the mechanical properties of SF was examined (Fig. 2). As expected RF combined with UVA light resulted in an increase in the Young's modulus of the SF matrices in a dose dependent manner. This is due to interfibrillar crosslinking brought on by RF. When added to collagen, RF has a significant effect on the fibrillogenesis kinetics under UVA, incrementing the materials stiffness [29]. Incremental increases in RF have also been shown to increase enzymatic degradation resistance of corneal tissue [30]. The addition of RA to SF had no significant effect on the Young's modulus.

When corneal stromal cells were seeded onto SF matrices, they attached more promptly on RF crosslinked matrices than controls (SF matrix) [Fig. 3(a)]. While there was a significant difference between RF crosslinked and non-crosslinked, the RF concentration used did not have a significant effect. After 5 h ~96% of cells attached on to the different 2.5 mM RF crosslinked SF matrices compared to ~85% attachment on SF alone. A similar pattern was recorded for different RA crosslinked SF matrices [Fig. 3(b)]. Cells adhered better onto RA crosslinked SF matrices (~83.5%) than control (~69%), 1 h after seeding. The variation in RA concentration did not lead to significant differences in cellular adhesion (~97%) over the 5 h following cell seeding. Significantly lower cellular adhesion was recorded for control matrix compared to RA crosslinked SF matrices ($p < 0.05$). One possible explanation for these results is that these bioactive molecules could have enhanced the expression of fibronectin or specific integrin receptor subunits [31] leading to better cellular adhesion [32].

Metabolic activity increased over 21 days for all matrix compositions, indicating an increase in proliferation. Metabolic activity was significantly higher for 2.5 mM RF crosslinked SF matrices after 21 days of culture compared to other concentration of RF crosslinked SF matrices ($p < 0.05$) and control ($p < 0.01$) [Fig. 3(c)]. This RF concentration is similar to that used in treatments involving corneal crosslinking – 2.66 mM [18]. Metabolic activity on 10 µM RA crosslinked SF matrices was significantly higher compared to other concentrations ($p < 0.01$) and the control group ($p < 0.01$) [Fig. 3(d)]. Although initially (up to day 3) there was no significant difference in metabolic activity between different concentrations of RA crosslinked SF matrices, by day 21 metabolic activity had increased for all compositions. These results suggest that the matrices were biocompatible.

To better understand these results, it is necessary to understand the mechanisms by which RF affects SF and RA affect cell behavior. RF acts as a photo sensitizer by producing free radicals (oxygen singlets), thus activating the natural lysyl oxidase pathway – similar to the collagen crosslinking pathway [33]. However, it is believed that the oxygen singlets more likely induce crosslinking not through lysyl oxidase but by production of imidazolone that attaches to certain molecules (e.g., histidine) forming fresh covalent bonds [34]. There is also triggering of the ECM's endogenous carbonyl groups that form crosslinks and RF's degradation that release 2,3-butanedione and that reacts with stromal protein endogenous carbonyl groups [34]. The overall result of these mechanisms is interfibrillar crosslinking and an increase in stiffness. Retinoic acid induces corneal stromal regeneration markers through both nuclear receptors mediated and nonnuclear receptor mediated pathways. Primarily, it binds to RA receptors (RAR) [35] that in turn act as transcription factors, binding to RA response elements (RARE) in the nucleus or to retinoic X receptors (RXR) causing either transcriptional activation of the target genes or repressing the retinoid-controlled genes.

While RF and RA have been shown to aid corneal regeneration, excess quantities of either of them can prove to be detrimental. RF exposed to UV light can alter physiochemical properties of the biopolymer it is crosslinking and may even affect the DNA of living cells on the material [36]. In the cornea, exposure to UVA light after the addition of RF leads to keratocyte apoptosis [37]. Similarly, excessive RA in cells leads to expression of disease-associated, mutated forms of Retinol Dehydrogenase 12 [38]. These concerns stress the need for optimized loading of both bioactive molecules. The mechanism used here of binding RF molecules into SF matrix follows a previous method [7]. Excited riboflavin molecules radicalize tyrosine residues that are on the silk chain, forming dityrosine complexes that in turn link up silk molecules. All trans RA molecules are covalently coupled with SF matrix by carbodiimide coupling reactions.

Following mechanical characterization and preliminary cellular evaluation concentration of 2.5 mM RF and 10 µM RA were chosen to be covalently coupled on SF matrices for further evaluation. Detailed, physical, mechanical and *in vitro* examinations were carried out with RF (2.5 mM) and RA (10 µM) and dual bioactive molecules (RF + RA) crosslinked SF matrices. Matrix with solely SF was used as a control for this study.

3.2. Physical, chemical and thermal characterization of RF and RA loaded SF matrices

The surface topography of the SF matrices was examined by SEM [Supplemental Fig. 1] and AFM [Fig. 4]. SEM showed a smooth flat surface with no visible defects or pores and no variation between samples at a micrometer range. EDS analysis of the fabricated matrices

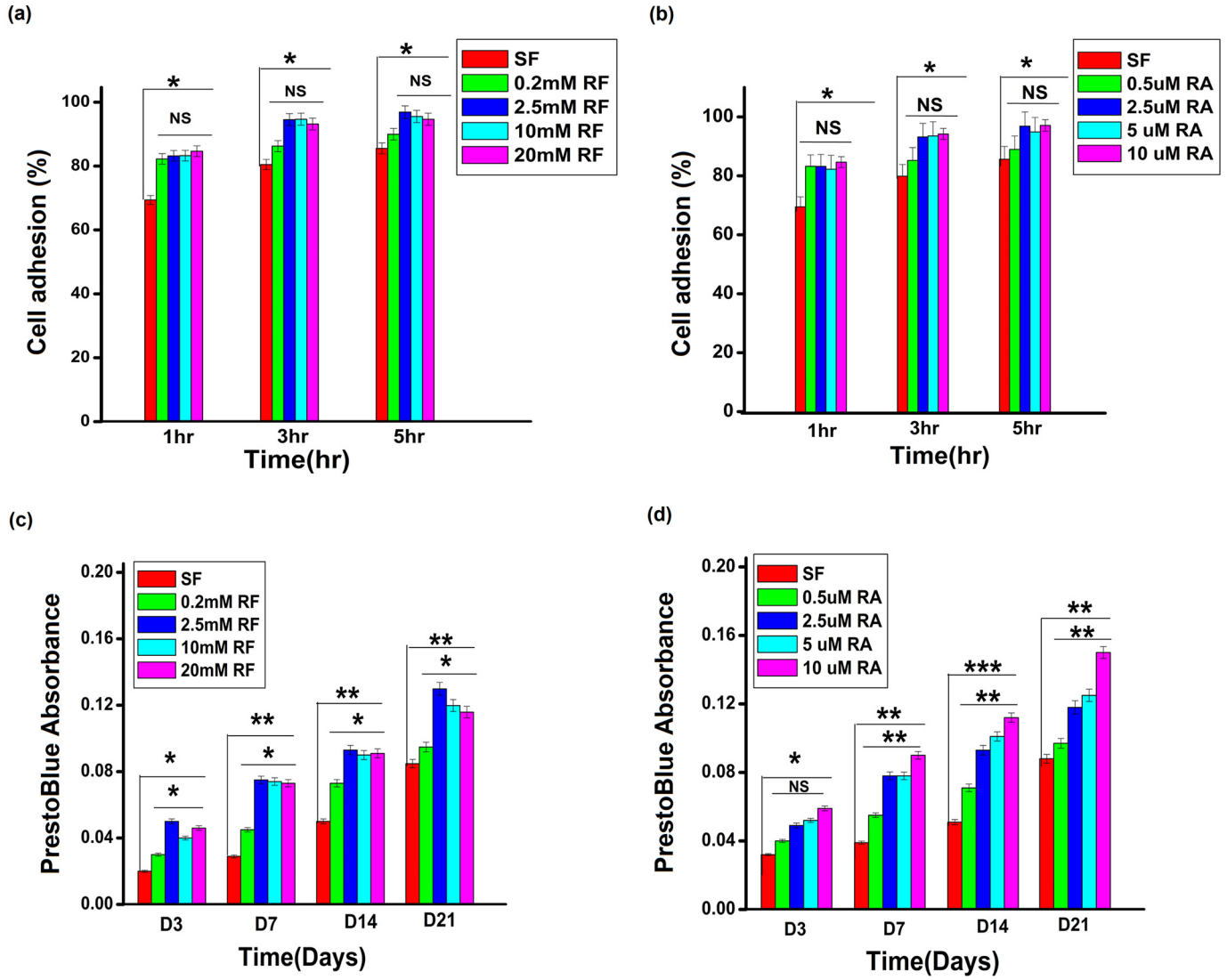

Fig. 3. Initial cell attachment efficiency on (a) different concentration of RF crosslinked SF matrices and (b) different concentration of RA loaded SF matrices. Total cell metabolism on (c) different concentration of RF crosslinked SF matrices (d) different concentration of RA loaded SF matrices evaluated by Presto-blue assay. ***p < 0.001, **p < 0.01 and *p < 0.05.

[Supplemental Fig. 1] showed that percentage nitrogen increased with the incorporation of bioactive molecules compared to the SF matrix. There were some differences in topography at a nanoscale as shown by AFM. The SF matrix surface was generally smooth with small single granules present resulting in a mean surface roughness (RMS) of 3.4 ± 0.6 nm. Loading of RF led the matrix to form oval shaped granules of lateral dimensions between 150 nm and 230 nm. They were randomly distributed over the surface, without forming any clusters. The RMS value for SF + RF matrix was 10.25 ± 0.45 nm. For SF + RA matrices, granular features were 80–250 nm and covered only a small portion of the matrix surface. The SF + RF + RA matrix topography was very similar to SF + RA with some aggregated granules forming clusters. The granules induced by intermolecular crosslinking of the RF surface were much larger than those formed on the surface of SF + RA and the aggregated granules were more regular and more densely grouped together. The RMS value recorded for SF + RA and SF + RF + RA were 14.87 ± 0.52 nm and 24.5 ± 0.86 nm, respectively. Nanoscale topographic features from the underlying substratum have been previously shown to directly affect cell behaviors, including adhesion, orientation, differentiation, migration, and proliferation [39–41]. Hence, the surface roughness of the different matrices could act as a contributing factor in modulating cell behavior. The average thickness of the matrix (n = 20) was calculated to be 35.2 ± 2.1 μm using a profilometer.

ATR-FTIR spectroscopy was used to compare the chemical composition of the different matrices [Fig. 5(a)]. Of the major vibration peaks detected, the following three vibration peaks associated with SF were identified: 1650–1630 cm^{-1} for amide I (C═O stretching), 1540–1520 cm^{-1} for amide-II (secondary NH bending, due to β-sheet structure), and 1270–1230 cm^{-1} for

amide III (C–N and N–H functionalities) [25]. Absorption peaks at ~1535 cm^{-1} and ~1648 cm^{-1} corresponded to the β-sheet structure (amide II). Protein conformation was confirmed from the presence of an amide I band, embodied by the C═O stretching vibration [42]. Hydrogen bond strength, for those between N–H and C═O groups, impacts the vibration frequency in the band. Protein backbone conformational structure controls bond strength [43]. The main vibrational frequencies of riboflavin in the spectral region lies between 1740 and 1100 cm^{-1} [44] since the C═O stretching of the carboxylic acid group of all-trans RA is in the range of 1720 cm^{-1} [45]. Loading of RF and RA on the SF matrix exhibited peak shift of the matrices. For RF crosslinked SF matrix, Amide *I* and II was shifted from 1646 cm^{-1} to 1600 cm^{-1} and 1534 cm^{-1} to 1500 cm^{-1} respectively. For RA coupled SF matrix, Amide *I* and II was shifted from 1646 cm^{-1} to 1619 cm^{-1} and

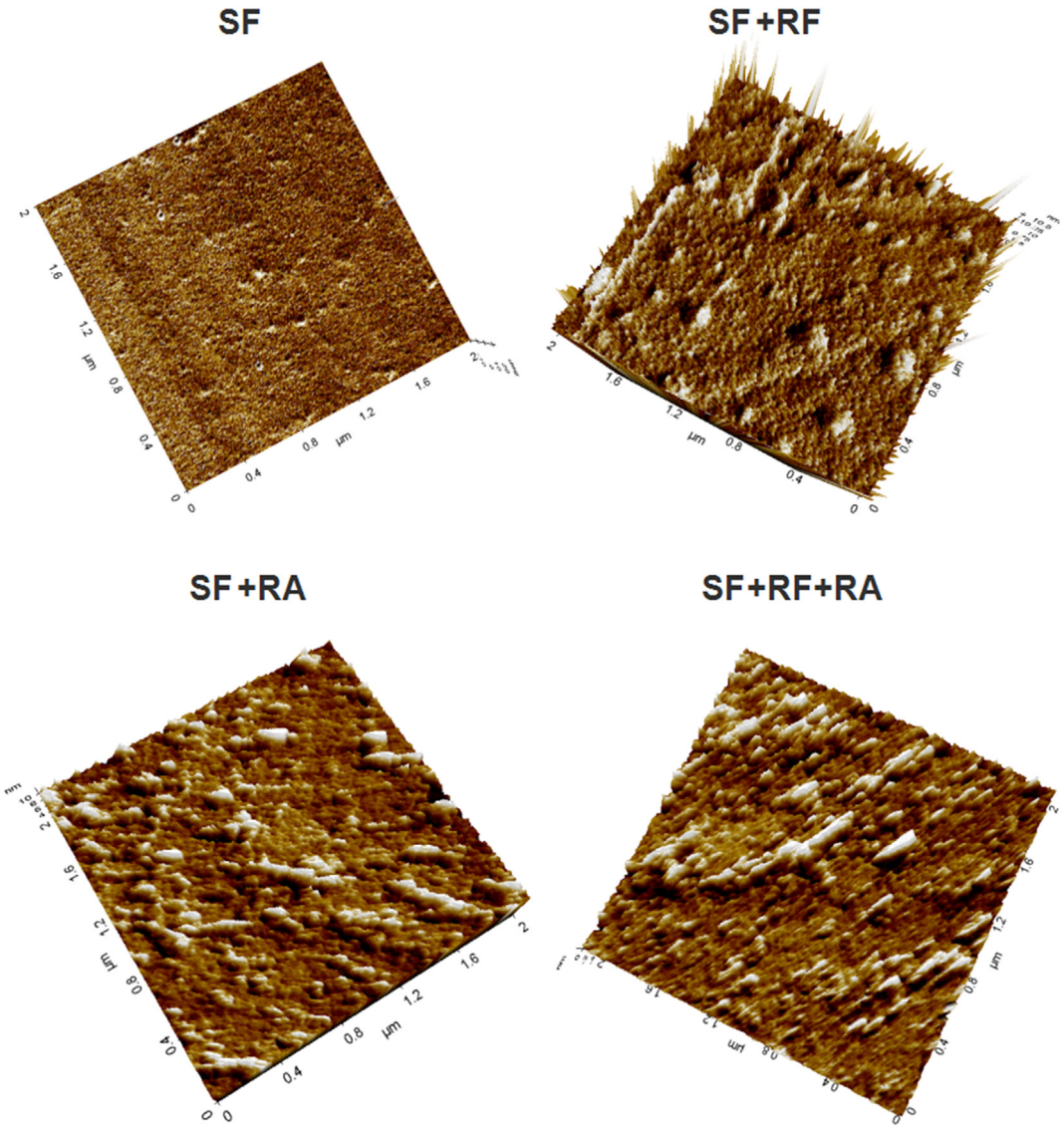

Fig. 4. AFM pictographs of different matrices show the surface topography (2 μm × 2 μm scan area). Surface roughness (Rq) was calculated from AFM images using Pico Image Basic Software.

1534 cm^{-1} to 1512 cm^{-1} respectively. This indicates the inclusion of bioactive molecules in the matrix without any major structural alteration. For both matrices, SF + RF and SF + RA, a few minor absorption peaks were observed in the range of 1740 cm^{-1} to 1100 cm^{-1}(indicated by blue dotted box in Fig. 5(a)). No strong peaks corresponding to RF and RA were observed on the spectra when overlapped with peaks corresponding to SF. FTIR spectra of dual bioactive molecule loaded matrices (SF + RF + RA) contained absorption peaks corresponding to SF and respective absorption peaks of RF and RA, without having undergo any major transformation or peak shift. This confirms structural stability of the matrices [46].

XRD patterns [Supplemental Fig. 2(a)] contained characteristics peaks associated with SF, RF and RA for the fabricated matrices. The XRD pattern for SF + RF matrix [Supplemental Fig. 2(b)] showed a decrease in the intensities of sharp peak of RF powder. Increased water content following crosslinking of the SF solution, resulted in a decrease in the intensities of sharp peak of RF. Dual bioactive molecule loaded matrix (SF + RF + RA) showed the corresponding peaks of SF, RF and RA. However, deconvolution and broadness of the peaks were recorded for single (SF + RF and SF + RA) and combined (SF + RF + RA) bioactive loaded matrices due to overlapping of peak positions.

The DSC thermograms of the matrices were represented in Supplemental Fig. 2(c). Pure silk fibroin exhibits a broad melting endotherm, over a temperature range of 250–350 °C. In the present study, the endotherm appeared at 289 °C. Melting temperatures for SF + RF, SF + RA and SF + RF + RA shifted to 279.6 °C, 268.4 °C and 273.8 °C respectively, indicating the effect of crosslinking and grafting with silk fibroin. However, no clear degradation peak ascribable to the silk fibroin was observed between 250 °C and 350 °C, for any of the compositions.

To function as a material to replace damage cornea, the matrices needs to have similar optical properties to a healthy cornea. The percentage transmittance of visible light through the matrices was between 80% and 95% with a decrease in transmittance once the light wavelength fell into the UV region [Fig. 5(b)]. The refractive index of the SF was calculated to be 1.45 ± 0.01. The addition of RF and RA made no significant difference to these properties. Both the light transmittance and the refractive index were similar to those found to human cornea [47].

The hydrophobic/hydrophilic nature of a substrate material affect its biocompatibility [25]. To determine the hydrophilicity of the matrices, the contact angle of a drop of water on the material was

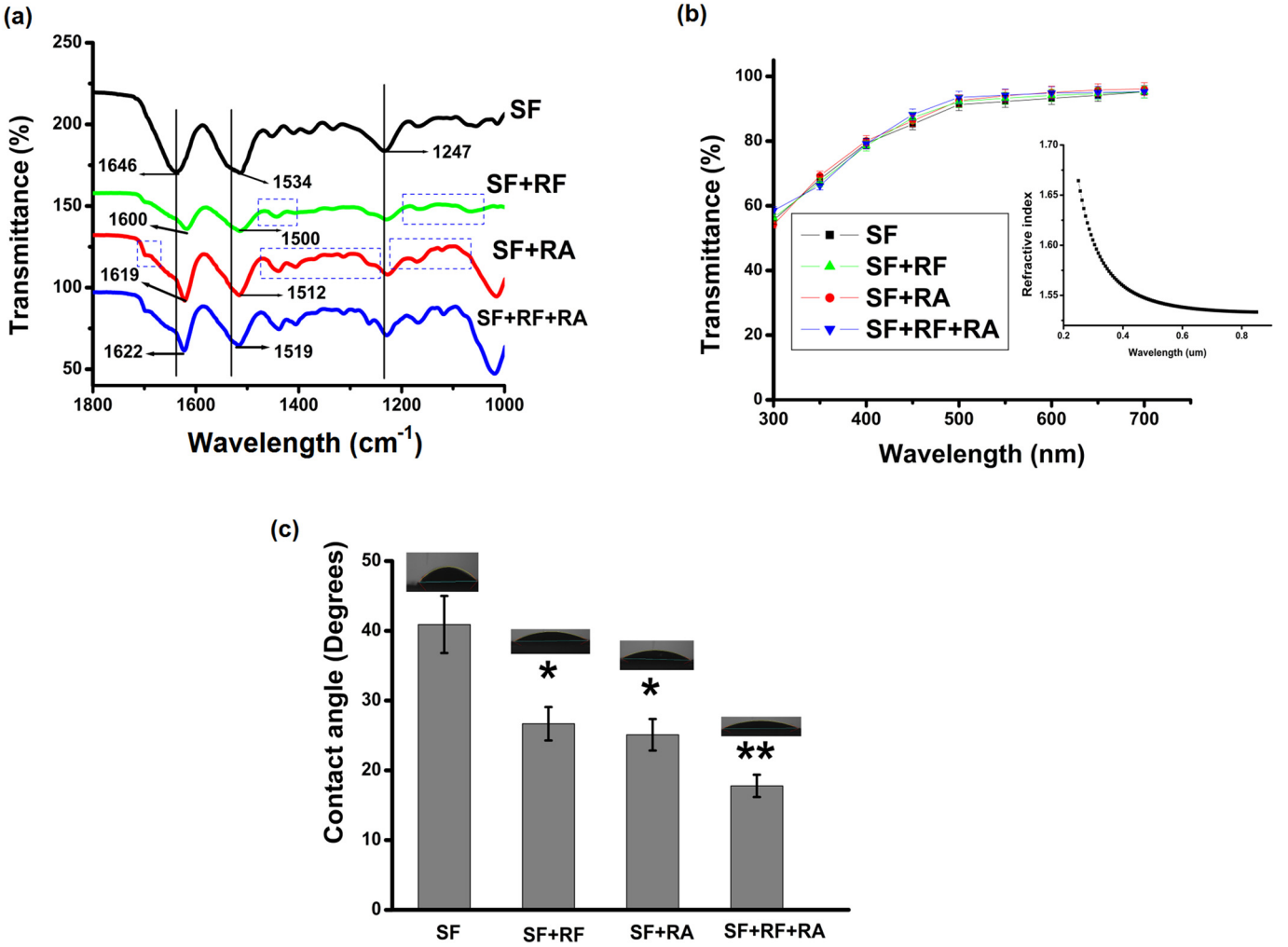

Fig. 5. (a) FTIR spectra of matrices. The dual bioactive molecule loaded matrix reveal peaks of corresponding to β sheet structure of SF and respective absorption peaks of RF and RA without any major alterations. (b) Light transmittance and refractive index of the matrices. (c) Hydrophilicity of different matrices. Loading of bioactive molecules significantly increased wettability of the matrices. ***p < 0.001, **p < 0.01 and *p < 0.05, n = 5 ± SD at each time point.

measured (n = 5) (Fig. 5(c)). The results show that incorporation of bioactive molecules, reduces the hydrophobicity of the SF matrix. The changes in surface roughness shown in Fig. 4 may in part explain this change. The hydrophilic changes to SF could also explain why there was an increase in cell adhesion after the addition of RF and RA molecules. Previous studies have shown a relationship between surface wetness and cell adhesion with hydrophilic materials displaying better adhesion than hydrophobic materials [48].

No significant distinction in Young's modulus [Fig. 6(a)] was recorded SF + RF + RA matrices compared to SF + RF matrices. This agrees with the data shown in Fig. 2 where the addition of RA had no effect on the mechanical properties of the matrices.

2.5 mM RF and 10 μM RA were loaded onto SF matrices via UV crosslinking and carbodiimide coupling reaction respectively. The controlled release kinetics for RF and RA loaded SF matrices in PBS, over 28 days is shown in Fig. 6(b). Cumulative release of bioactive molecules normalized to the amount of each molecule present in the matrices was calculated. A burst release was observed over the first 3 days, for both molecules. This may be due to release of non-conjugated, physically adsorbed or loosely bound bioactive molecules. These molecules would have been retained during the rinsing steps. Following the burst release, there was a sustained release of both bioactive molecules up to day 14 after with no further release was detectable. Approximately 29% of the RF and 40% of the RA were released from the SF matrix. The sustained release of bioactive molecules may be due to strong bonding between functional groups of bioactive molecules and silk fibroin.

To understand the mechanism of release for bioactive molecules incorporates into the scaffolds, the structure of SF film needed to be considered. Release of RA from SF was higher than that of RF. SF has two forms (termed Silk I and II) where Silk II has a semi-crystalline structure with crystals being dispersed across the amorphous, continues matrix of Silk I [49]. The sustained release of biomolecules embedded in SF is dependent on the location of these molecules. Molecules may remain in the space between β-sheets in the crystalline or nano-crystalline region. While Silk II is a stable structure, silk I has been known to swell in aqueous environments [50] resulting in the silk matrix swelling. A concentration gradient causes molecules in the nano-crystalline region to release. The release is sustained by Silk II crystals and the amorphous, polypeptide chain. The hindrance from the amorphous polypeptide chain and increasing free space in the amorphous region in-between the Silk II crystals can contribute to the sharp drug release [50]. Following this sharp change, caused by gradual acclimatization to the aqueous environment, the release rate stabilize to an equilibrium lasting until day point 28. Similar release profiles have been observed for other molecules embedded in silk fibroin matrices [51].

Treatment with the enzyme proteinase K over 21 days results in a time dependent decrease in dry weight (49% loss of dry weight for SF, 58.23% for SF + RF, 52.17% for SF + RA and 55% for SF + RF + RA [Fig. 6(c)]). There was no noticeable difference in the degradation rate

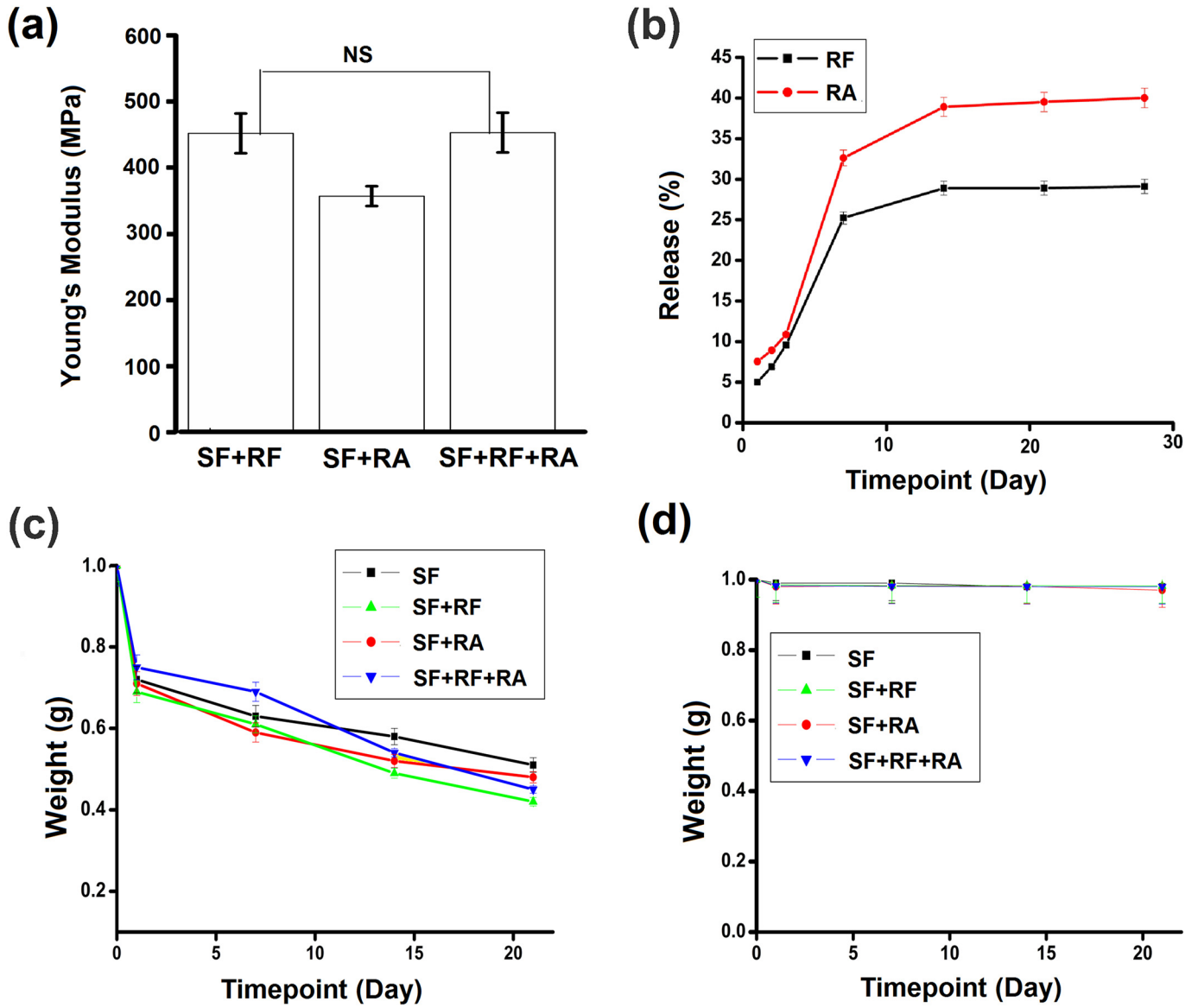

Fig. 6. (a) Young's modulus of single (2.5 mM RF and 10 μM RA) and dual (2.5 mM RF + 10 μM RA) bioactive molecule loaded SF matrices. (b) Controlled release kinetics of RF and RA from SF matrices. The degradation of matrices at 37 °C in (c) proteinase K (Tritirachium album) solution or (d) buffer solution (PBS, pH 7.4). The extent of degradation was expressed in terms of weight remaining at each time point.

following the incorporation of RF or RA. When submerged in the control PBS solution (pH 7.4), none of the matrices had any notable weight loss [Fig. 6(d)]. Moderate biodegradation can be an important asset for materials used to form scaffolds. It can influence cell growth and viability as well as the host response [52]. Ideally, the *in vivo* degradation rate of the material should match the rate of new tissue formation. Silk-based matrix degradation, through proteinase K, has some similarities to the degradation produced by some typical human enzymes [53].

3.3. Cell behavior on RF and RA loaded SF matrices

Corneal stromal cells more promptly attached onto bioactive molecules loaded SF matrices, compared to control matrices [Fig. 7(a)]. Within the first hour, approximately 63%, 82%, 84% and 85% of cells had attached onto SF, SF + RF, SF + RA and SF + RF + RA matrices respectively. There was no significant difference in cellular adhesion between SF + RF, SF + RA and the dual loaded SF + RF + RA matrices 5 h after seeding. Increased nanoscale surface roughness of these matrices is likely to have led to greater adsorption of adhesive molecules [25] and also increased surface hydrophilicity, thus leading to improved cell adherence. Cells that adhered well upon matrices are more likely to form an organized ECM [54] which is vital for successful tissue regeneration.

Cell metabolism was significantly higher ($p < 0.01$) for cells on SF + RF + RA matrices, compared to SF + RF and SF + RA matrices [Fig. 7(b)]. There was no significant difference between cells on SF + RF and SF + RA matrices up to 21 days of culture. Toxicity assays (MTT) indicated the absence of cytotoxicity on the fabricated matrices [Fig. 7(c)]. UVA mediated crosslinking (specifically for SF + RF and SF + RF + RA matrices) is hence unlikely to have generated any cytotoxic by-products in this study. All bioactive molecules loaded matrices were significantly higher when compared with control (SF matrix) at all day points. However, cells displayed a slow rate of proliferation over the total culture period on all matrices, most likely due to the use of low glucose, serum-free media. It has been demonstrated that low glucose conditions allow human corneal stromal cells to survive for long periods in culture while also retaining their keratocyte-characteristic phenotype in serum-free conditions [55]. It should

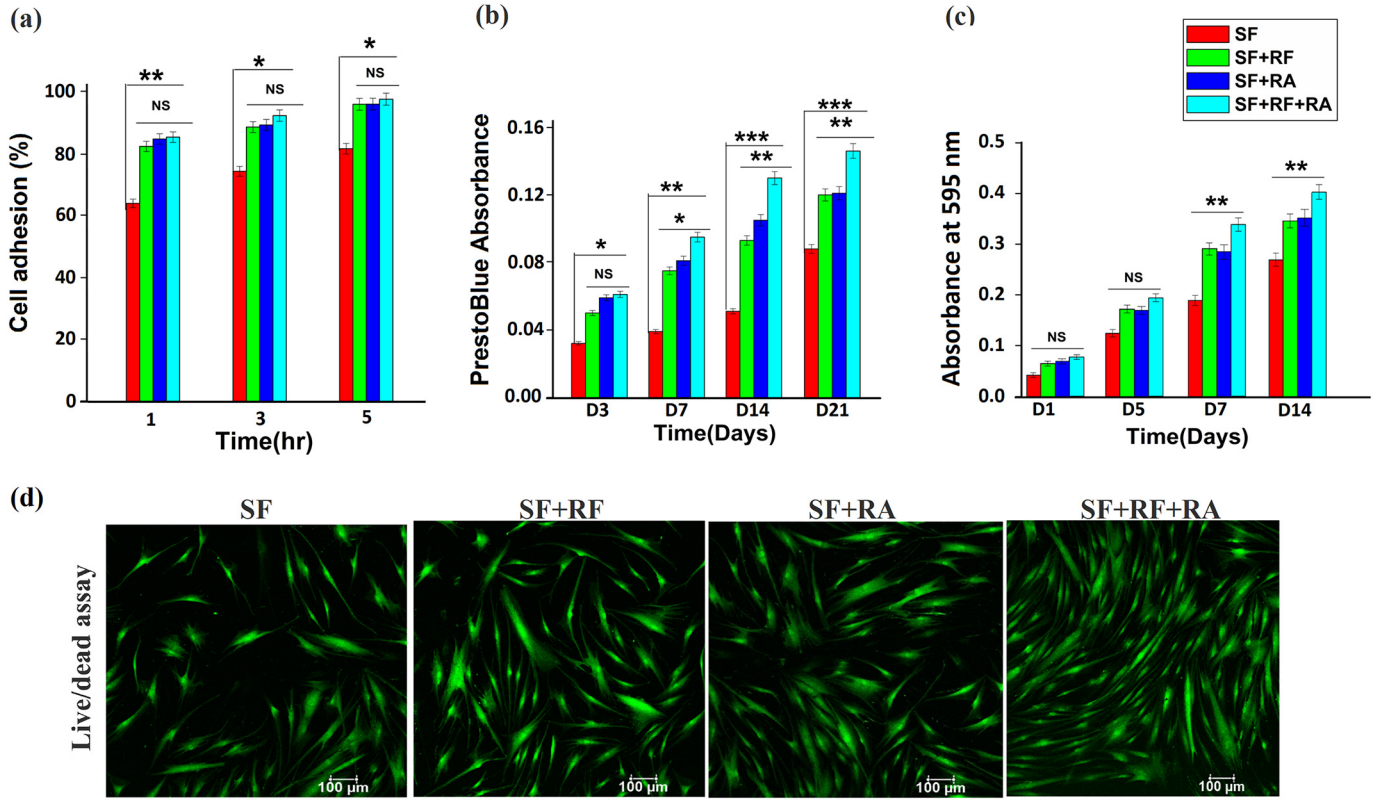

Fig. 7. (a) Initial cell attachment efficiency, (b) total cell metabolism and (c) toxicity of cells on single (SF + RF, SF + RA) and dual (SF + RF + RA) bioactive molecule loaded SF matrices. ***p < 0.001, **p < 0.01 and *p < 0.05. (d) Viability of cells on different matrices using live/dead assay (live cells appear green and dead cells appear red) imaged using confocal microscopy on day 7. Scale bar = 100 µm. (For interpretation of the references to color in this figure legend, the reader is referred to the web version of this article.)

also be noted that metabolic activity data could be influenced by the initial cell adhesion although the difference in metabolism between groups are much larger than the differences in cell adhesion. No difference in the trend of cellular metabolism activity was recorded for any of the composition, with either the higher or the lower cell concentration [Supplemental Fig. 3].

The viability of cells on different matrices was examined using live/dead staining assay [Fig. 7(d)]. Cells cultured on all matrices remained viable with no dead cells present, implying non-cytotoxicity of the matrices. There appears to be more cells present on SF + RF + RA matrices, followed by SF + RA and SF + RF matrices and then the control SF matrix. This would appear to correlate with the results from the metabolic activity assay and suggest that SF + RF + RA matrices are the most effective at supporting cell proliferation.

The organization of a cells cytoskeleton plays an important role in modulating cell adhesion, migration and matrix contractibility. There appear to be an increase in actin stress fibers present in cells on bioactive molecules loaded matrices (SF + RF, SF + RA and SF + RF + RA) compared to controls (SF) as shown in Fig. 8(a). Upon the control matrix, actin distribution was sparse and uneven, being limited to the immediate vicinity of the cell and the cells themselves were also fewer in number. Matrices with bioactive molecule also had increased vinculin localization at focal adhesions compared to controls, indicating better cell attachment as shown in Fig. 8(b). Focal adhesions connect the cell cytoskeleton to the extracellular matrix and play an important role in regulating cell migration and intracellular signaling processes [56,57]. Quantification of cellular shape was presented in Supplemental Fig. 2(d). There is no significant difference in cell shape (with respect of aspect ratio) between single (SF + RF and SF + RA) and dual bioactive molecule loaded (SF + RF + RA) matrices. A significantly (*p < 0.05) lower aspect ratio was recorded for only SF matrix and less stress actin was observed after 14 days of culture (Fig. 8a). Total cell density per unit square area for SF (~4 cells/unit square), SF + RF (~9 cells/unit square), SF + RA (~11 cells/unit square) and SF + RF + RA (~19 cells/unit square) was calculated from the images.

Markers associated with keratocyte and myofibroblastic phenotypes were evaluated by immunofluorescent staining [Fig. 9]. Keratocyte markers ALDH3A1 and keratocan were present in cells on all matrices. αSMA, a myofibrotic marker, was not detected on SF, SF + RF or SF + RA matrices. However, αSMA was detected in small numbers of cells on the combined bioactive molecule loaded matrices.

Gene expression of several keratocyte markers was evaluated using rtPCR after 14 and 28 days of culture. Addition of bioactive molecules significantly increased the expression of ALDH3A1, keratocan, decorin and lumican by day 28 [Fig. 10]. ALDH3A1 expression was significantly increased for SF + RF, SF + RA and SF + RF + RA (10.2 ± 0.71, 12.52 ± 1.001 and 17.52 ± 1.22–fold increase, respectively) when compared to SF alone at day 28 (6.23 ± 0.43–fold increase). A significant increase in keratocan was demonstrated for SF + RF, SF + RA and SF + RF + RA (24.52 ± 0.714, 21.57 ± 1.0016 and 27.89 ± 1.26–fold increase, respectively) compared to SF alone (15.98 ± 0.44–fold increase). Significant increments for decorin and lumican were also recorded for all bioactive molecule loaded matrices, compared to control. Expression of all keratocyte markers were significantly increased for all compositions from day 14 to day 28. Expression of collagen type I, III and V, the most abundant collagens in the corneal stroma, were also assessed. Collagen type I, type III and type V expression was significantly enhanced by day 28 for SF + RF (~7.52,~6.79 and ~4.47 -fold increase respectively), SF + RA (~8.54, ~5.98 and~4.86 -fold increase respectively) and SF + RF + RA (~11.52,~9.9 and ~7.18 -fold increase respectively) compared to

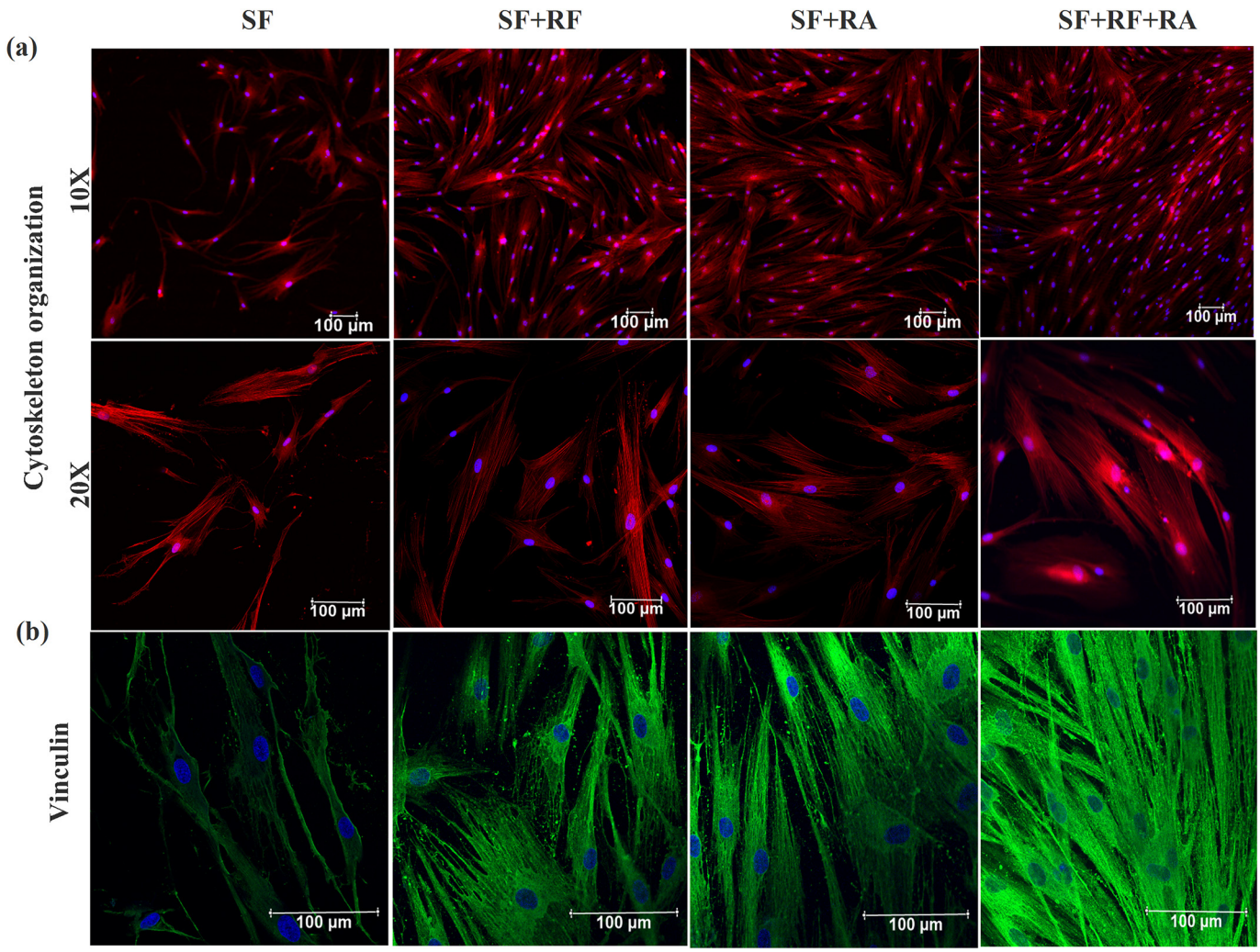

Fig. 8. Confocal images of corneal stromal cells after 14 days in culture after staining (a) actin filaments (red) and nuclei (blue) or (b) vinculin (green) and nuclei (blue). Scale bar = 100 µm. (For interpretation of the references to color in this figure legend, the reader is referred to the web version of this article.)

~3.2,~2.5 and ~2.48–fold increase in the SF matrix. The increased expression of these proteins should lead to improved matrix deposition, which is vital for tissue formation.

αSMA (ACTA2) gene expression, revealed that SF + RF (~0.32 and ~1.2–fold decrease), SF + RA (~0.5 and ~1.48–fold decrease) and SF + RF + RA (~0.39 and ~1.29–fold decrease) had significantly lower expression than SF (~0.52 and ~0.47–fold increase) at day 14 and day 28 respectively [Fig. 9]. When combined with the results from immunocytochemical staining, it is clear that myofibroblastic differentiation was limited on all the SF matrices. Only SF + RF + RA group contained a small population of cells that stained positive for αSMA. This result is similar to those presented in some previous studies that also found a small percentage of cells staining positive for αSMA when cultured in RA supplemented serum free media [58] and RA resulting in a small increase in αSMA expression [59,60]. Some corneal stroma cells may have become myofibroblastic during their expansion in serum prior to being placed onto the matrices and it is probably that some of these cells remained viable when cultured serum free on SF + RF + RA. UVA aided riboflavin cross-linking of cornea was previously shown to positively stain keratocytes for CD34 but remain negative for αSMA [61].

To generate corneal tissue, cells are required to synthesize and secrete corneal specific ECM. In corneal stromal ECM, the most common, negatively charged macromolecules are the glycosaminoglycan (GAG) polysaccharides. These are normally covalently attached to proteoglycan core proteins and make vital contributions towards corneal transparency, cell adhesion, and nerve growth cone guidance [62]. Quantification of GAG synthesis for cells on SF + RF (~5.22 µg), SF + RA (~5.01 µg) and SF + RF + RA (~7.09 µg) matrices demonstrated that significantly more GAG was present when compared to SF (~2.85 µg) at day 28 [Fig. 11(a)]. A similar trend was present when the GAG was normalized to the DNA present at day 14 and 28 [Fig. 11(b)]. No significant increment of GAG production (normalized to DNA) was recorded for the SF matrix from day 14 to day 28. Previous studies have shown that both RF [62] and RA [63] stimulate cell proliferation and the release of hyaluronic acid, a GAG that has a role in corneal wound healing. In addition, GAGs such as chondroitin sulphate and keratan sulphate are necessary to control inter-fibril spacing and corneal transparency [64].

Since the focus of this study was to examine the effect that incorporating biomolecules into SF had on corneal stromal cells rather than directly developing a scaffold that is immediately implantable, some modifications to the matrices are likely to be required prior to their use *in vivo*. Since no pores were visible via SEM, we expect that cells can only migrate over the matrix surface rather than through them. Pores could be incorporated into the matrices via techniques such as solvent casting [65] or electrospinning [66]. Alternatively, since the matrices are very thin, once cells are confluent on the matrix, multiple layers could be stacked upon each other to generate a 3D engineered stroma.

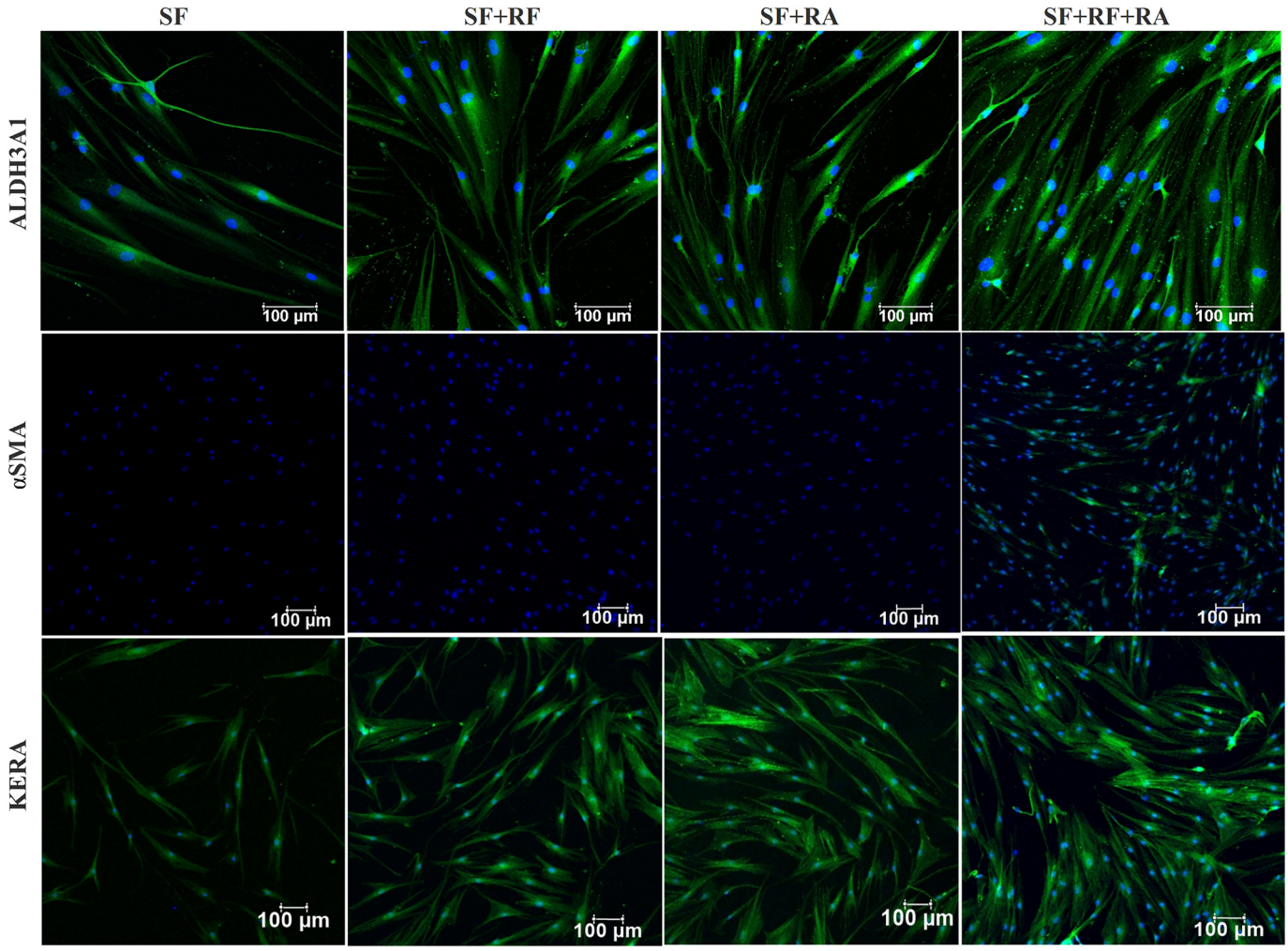

Fig. 9. Immunofluorescent staining of protein markers ALDH3A1, αSMA and keratocan, (all green) and nuclei (blue) after 14 days in culture. Scale bar = 100 μm. (For interpretation of the references to color in this figure legend, the reader is referred to the web version of this article.)

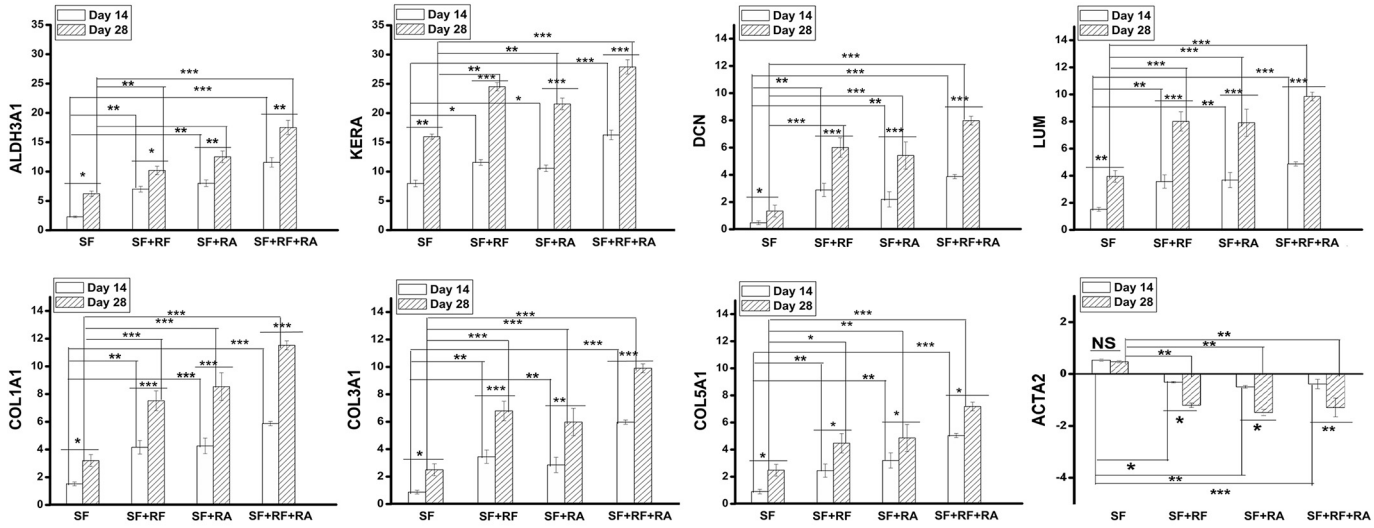

Fig. 10. Fold change gene expression analysis of corneal keratocyte-specific markers ALDH3A1, KERA, DCN and LUM; extracellular matrix markers COL1A1, COL3A1, COL5A1 and myofibroblastic marker αSMA as quantified by rtPCR. Gene expression is normalized to GAPDH. ***$p < 0.001$, **$p < 0.01$ and *$p < 0.05$.

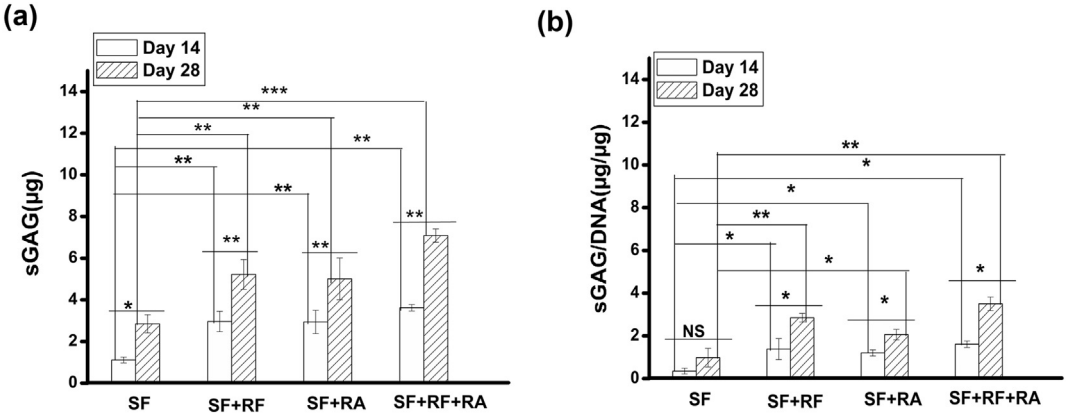

Fig. 11. (a) Combined sGAG production in construct and culture media as quantified by DMMB assay; (b) ratio of sGAG/DNA present after 14 and 28 days. ***p < 0.001, **p < 0.01 and *p < 0.05.

The culmination of all these observations strongly favors the strategy of dual bioactive molecule loading as an attractive option, suitable for further explorations in corneal stromal regeneration. Further improvements can be achieved by optimizing the quantity, delivery rate and mode, and proportion of the molecules. In addition, these molecules have the potential to be incorporated into different types of SF scaffolds.

4. Conclusion

In the present study, it has been demonstrated that the covalently coupling of bioactive molecules together (Riboflavin and all-trans Retinoic acid) into silk fibroin matrix positively influence corneal stromal cell behavior. The findings from detailed *in vitro* studies show that combined loading of bioactive molecules was better at supporting cell adhesion, proliferation, ECM formation, and keratocyte-associated gene expression. This confirms our hypothesis regarding the use of a combination of bioactive molecules to generate a suitable matrix for corneal regeneration. Further studies will examine the incorporation of multiple regulatory signals, stemming from growth factors, into cell-based tissue engineering systems that promise to open doors towards more potent and productive corneal tissue regeneration therapies.

Supplementary data to this article can be found online at https://doi.org/10.1016/j.msec.2019.110093.

Acknowledgements

The research leading to these results has received funding from the European Research Council (ERC) under the European Union's Horizon 2020 research and innovation program (EYEREGEN - 637460) and from Science Foundation Ireland (15/ERC/3269).

Declaration of competing interest

Authors have no conflict of interest.

References

[1] M. Oliva, M. Gulati, T. Schottman, Turning the tide of corneal blindness, Indian J. Ophthalmol. 60 (2012) 423, https://doi.org/10.4103/0301-4738.100540.
[2] A.L. Yu, M. Kaiser, M. Schaumberger, E. Messmer, D. Kook, U. Welge-Lussen, Donor-related risk factors and preoperative recipient-related risk factors for graft failure, Cornea 33 (2014) 1149–1156, https://doi.org/10.1097/ICO.0000000000000225.
[3] P. Gain, R. Jullienne, Z. He, M. Aldossary, S. Acquart, F. Cognasse, G. Thuret, Global survey of corneal transplantation and eye banking, JAMA Ophthalmol 134 (2016) 167–173, https://doi.org/10.1001/jamaophthalmol.2015.4776.
[4] H. Tao, D.L. Kaplan, F.G. Omenetto, Silk materials - a road to sustainable high technology, Adv. Mater. 24 (2012) 2824–2837, https://doi.org/10.1002/adma.201104477.
[5] D. Ma, Y. Wang, W. Dai, Silk fibroin-based biomaterials for musculoskeletal tissue engineering, Mater. Sci. Eng. C. 89 (2018) 456–469, https://doi.org/10.1016/j.msec.2018.04.062.
[6] L.D. Koh, J. Yeo, Y.Y. Lee, Q. Ong, M. Han, B.C.K. Tee, Advancing the frontiers of silk fibroin protein-based materials for futuristic electronics and clinical wound-healing (invited review), Mater. Sci. Eng. C. 86 (2018) 151–172, https://doi.org/10.1016/j.msec.2018.01.007.
[7] M.B. Applegate, B.P. Partlow, J. Coburn, B. Marelli, C. Pirie, R. Pineda, D.L. Kaplan, F.G. Omenetto, Photocrosslinking of silk fibroin using riboflavin for ocular prostheses, Adv. Mater. 28 (2016) 2417–2420, https://doi.org/10.1002/adma.201504527.
[8] S. Wang, C.E. Ghezzi, R. Gomes, R.E. Pollard, J.L. Funderburgh, D.L. Kaplan, In vitro 3D corneal tissue model with epithelium, stroma, and innervation, Biomaterials 112 (2017) 1–9, https://doi.org/10.1016/j.biomaterials.2016.09.030.
[9] B.D. Lawrence, J.K. Marchant, M.A. Pindrus, F.G. Omenetto, D.L. Kaplan, Silk film biomaterials for cornea tissue engineering, Biomaterials 30 (2009) 1299–1308, https://doi.org/10.1016/j.biomaterials.2008.11.018.
[10] L.J. Bray, K.A. George, S.L. Ainscough, D.W. Hutmacher, T.V. Chirila, D.G. Harkin, Human corneal epithelial equivalents constructed on Bombyx mori silk fibroin membranes, Biomaterials 32 (2011) 5086–5091, https://doi.org/10.1016/j.biomaterials.2011.03.068.
[11] J. Wu, J. Rnjak-Kovacina, Y. Du, M.L. Funderburgh, D.L. Kaplan, J.L. Funderburgh, Corneal stromal bioequivalents secreted on patterned silk substrates, Biomaterials 35 (2014) 3744–3755, https://doi.org/10.1016/j.biomaterials.2013.12.078.
[12] J.L. Whittaker, N.R. Choudhury, N.K. Dutta, A. Zannettino, Facile and rapid ruthenium mediated photo-crosslinking of Bombyx mori silk fibroin, J. Mater. Chem. B 2 (2014) 6259–6270, https://doi.org/10.1039/c4tb00698d.
[13] H.A. Wee, P.J. Dyson, Classical and non-classical ruthenium-based anticancer drugs: towards targeted chemotherapy, Eur. J. Inorg. Chem. (2006) 4003–4018, https://doi.org/10.1002/ejic.200600723.
[14] Y. Zhang, P. Sukthankar, J.M. Tomich, G.W. Conrad, Effect of the synthetic NC-1059 peptide on diffusion of riboflavin across an intact corneal epithelium, Investig. Ophthalmol. Vis. Sci. 53 (2012) 2620–2629, https://doi.org/10.1167/iovs.12-9537.
[15] E.B. Masurovsky, E.R. Peterson, Photo-reconstituted collagen gel for tissue culture substrates, Exp. Cell Res. 76 (1973) 447–448, https://doi.org/10.1016/0014-4827(73)90399-6.
[16] S. Ibusuki, G.J. Halbesma, M.A. Randolph, R.W. Redmond, I.E. Kochevar, T.J. Gill, Photochemically cross-linked collagen gels as three-dimensional scaffolds for tissue engineering, Tissue Eng. 13 (2007) 1995–2001, https://doi.org/10.1089/ten.2006.0153.
[17] M. Ahearne, A. Coyle, Application of UVA-riboflavin crosslinking to enhance the mechanical properties of extracellular matrix derived hydrogels, J. Mech. Behav. Biomed. Mater. 54 (2016) 259–267, https://doi.org/10.1016/j.jmbbm.2015.09.035.
[18] S.H. Kim, C.C. Chu, Fabrication of a biodegradable polysaccharide hydrogel with riboflavin, vitamin B2, as a photo-initiator and L-arginine as coinitiator upon UV irradiation, J. Biomed. Mater. Res. - Part B Appl. Biomater. 91 (2009) 390–400, https://doi.org/10.1002/jbm.b.31414.
[19] A.K. Nguyen, S.D. Gittard, A. Koroleva, S. Schlie, A. Gaidukeviciute, B.N. Chichkov, R.J. Narayan, Two-photon polymerization of polyethylene glycol diacrylate scaffolds with riboflavin and triethanolamine used as a water-soluble photoinitiator, Regen. Med. 8 (2013) 725–738, https://doi.org/10.2217/rme.13.60.
[20] F.Z. Abidin, R.M. Gouveia, C.J. Connon, Application of retinoic acid improves form and function of tissue engineered corneal construct, Organogenesis 11 (2015) 122–136, https://doi.org/10.1080/15476278.2015.1093267.
[21] G. Duester, Keeping an eye on retinoic acid signaling during eye development, Chem. Biol. Interact. 178 (2009) 178–181, https://doi.org/10.1016/j.cbi.2008.09.004.
[22] R.M. Gouveia, C.J. Connon, The effects of retinoic acid on human corneal stromal keratocytes cultured in vitro under serum-free conditions, Investig. Opthalmology Vis. Sci. 54 (2013) 7483, https://doi.org/10.1167/iovs.13-13092.

[23] A.P. Lynch, M. Ahearne, Retinoic acid enhances the differentiation of adipose-derived stem cells to keratocytes in vitro, Transl. Vis. Sci. Technol. 6 (2017) 6, https://doi.org/10.1167/tvst.6.1.6.
[24] A.P. Lynch, F. O'Sullivan, M. Ahearne, The effect of growth factor supplementation on corneal stromal cell phenotype in vitro using a serum-free media, Exp. Eye Res. 151 (2016) 26–37, https://doi.org/10.1016/j.exer.2016.07.015.
[25] P. Bhattacharjee, D. Naskar, H.W. Kim, T.K. Maiti, D. Bhattacharya, S.C. Kundu, Non-mulberry silk fibroin grafted PCL nanofibrous scaffold: promising ECM for bone tissue engineering, Eur. Polym. J. 71 (2015) 490–509, https://doi.org/10.1016/j.eurpolymj.2015.08.025.
[26] A.M. Abd El-Hay, A.M. Naser, A. Badawi, M.A. Abd El-Ghaffar, H. Abd El-Wahab, D.A. Helal, Biodegradable polymeric microcapsules for sustained release of riboflavin, Int. J. Biol. Macromol. 92 (2016) 708–714, https://doi.org/10.1016/j.ijbiomac.2016.07.076.
[27] M. Ahearne, J. Lysaght, A.P. Lynch, Combined influence of basal media and fibroblast growth factor on the expansion and differentiation capabilities of adipose-derived stem cells, Cell Regen 3 (2014) 3:13, https://doi.org/10.1186/2045-9769-3-13.
[28] M. Ahearne, Y. Liu, D.J. Kelly, Combining freshly isolated chondroprogenitor cells from the infrapatellar fat pad with a growth factor delivery hydrogel as a putative single stage therapy for articular cartilage repair, Tissue Eng. Part A. 20 (2014) 930–939, https://doi.org/10.1089/ten.tea.2013.0267.
[29] M. Ahearne, Y. Yang, K.Y. Then, K.K. Liu, Non-destructive mechanical characterisation of UVA/riboflavin crosslinked collagen hydrogels, Br. J. Ophthalmol. 92 (2008) 268–271, https://doi.org/10.1136/bjo.2007.130104.
[30] N.A.L. O'Brart, D.P.S. O'Brart, N.H. Aldahlawi, S. Hayes, K.M. Meek, An investigation of the effects of riboflavin concentration on the efficacy of corneal cross-linking using an enzymatic resistance model in porcine corneas, Investig. Ophthalmol. Vis. Sci. 59 (2018) 1058–1065, https://doi.org/10.1167/iovs.17-22994.
[31] A.K. Shah, J. Lazatin, R.K. Sinha, T. Lennox, N.J. Hickok, R.S. Tuan, Mechanism of BMP-2 stimulated adhesion of osteoblastic cells to titanium alloy, Biol. Cell. 91 (1999) 131–142, https://doi.org/10.1016/S0248-4900(99)80037-9.
[32] S.I. Aota, M. Nomizu, K.M. Yamada, The short amino acid sequence Pro-His-Ser-Arg-Asn in human fibronectin enhances cell-adhesive function, J. Biol. Chem. 269 (1994) 24756–24761.
[33] G. Wollensak, E. Spoerl, T. Seiler, Riboflavin/ultraviolet-A-induced collagen crosslinking for the treatment of keratoconus, Am J. Ophthalmol. 135 (2003) 620–627, https://doi.org/10.1016/S0002-9394(02)02220-1.
[34] A. Scott McCall, S. Kraft, H.F. Edelhauser, G.W. Kidder, R.R. Lundquist, H.E. Bradshaw, Z. Dedeic, M.J.C. Dionne, E.M. Clement, G.W. Conrad, Mechanisms of corneal tissue cross-linking in response to treatment with topical riboflavin and Long-Wavelength Ultraviolet Radiation (UVA), Investig. Ophthalmol. Vis. Sci. 51 (2010) 129–138, https://doi.org/10.1167/iovs.09-3738.
[35] L.J. Gudas, J.A. Wagner, Retinoids regulate stem cell differentiation, J. Cell. Physiol. 226 (2011) 322–330, https://doi.org/10.1002/jcp.22417.
[36] W.T. Speck, C.C. Chen, H.S. Rosenkranz, In vitro studies of effects of light and riboflavin on DNA and HeLa cells, Pediatr. Res. 9 (1975) 150–153, https://doi.org/10.1203/00006450-197503000-00009.
[37] G. Wollensak, E. Spoerl, M. Wilsch, T. Seiler, Keratocyte apoptosis after corneal collagen cross-linking using riboflavin/UVA treatment, Cornea 23 (2004) 43–49, https://doi.org/10.1097/00003226-200401000-00008.
[38] S.A. Lee, O.V. Belyaeva, I.K. Popov, N.Y. Kedishvili, Overproduction of bioactive retinoic acid in cells expressing disease-associated mutants of retinol dehydrogenase 12, J. Biol. Chem. 282 (2007) 35621–35628, https://doi.org/10.1074/jbc.M706372200.
[39] S.J. Liliensiek, S. Campbell, P.F. Nealey, C.J. Murphy, The scale of substratum topographic features modulates proliferation of corneal epithelial cells and corneal fibroblasts, J. Biomed. Mater. Res. - Part A. 79 (2006) 185–192, https://doi.org/10.1002/jbm.a.30744.
[40] L.A. Turner, M. J. Dalby, Nanotopography-potential relevance in the stem cell niche, Biomater. Sci. 2 (2014) 1574–1594, https://doi.org/10.1039/c4bm00155a.
[41] E.K.F. Yim, E.M. Darling, K. Kulangara, F. Guilak, K.W. Leong, Nanotopography-induced changes in focal adhesions, cytoskeletal organization, and mechanical properties of human mesenchymal stem cells, Biomaterials 31 (2010) 1299–1306, https://doi.org/10.1016/j.biomaterials.2009.10.037.
[42] D.M. Byler, H. Susi, Examination of the secondary structure of proteins by deconvolved FTIR spectra, Biopolymers 25 (1986) 469–487, https://doi.org/10.1002/bip.360250307.
[43] O.N. Tretinnikov, Y. Tamada, Influence of casting temperature on the near-surface structure and wettability of cast silk fibroin films, Langmuir 17 (2001) 7406–7413, https://doi.org/10.1021/la010791y.
[44] M.M.N. Wolf, C. Schumann, R. Gross, T. Domratcheva, R. Diller, Ultrafast infrared spectroscopy of riboflavin: dynamics, electronic structure, and vibrational mode analysis, J. Phys. Chem. B 112 (2008) 13424–13432, https://doi.org/10.1021/jp804231c.
[45] T.K. Maiti, K.S. Ghosh, J. Debnath, S. Dasgupta, Binding of all-trans retinoic acid to human serum albumin: fluorescence, FT-IR and circular dichroism studies, Int. J. Biol. Macromol. 38 (2006) 197–202, https://doi.org/10.1016/j.ijbiomac.2006.02.015.
[46] Y. Tamada, New process to form a silk fibroin porous 3-D structure, Biomacromolecules 6 (2005) 3100–3106, https://doi.org/10.1021/bm050431f.
[47] K.M. Meek, C. Knupp, Corneal structure and transparency, Prog. Retin. Eye Res. 49 (2015) 1–16, https://doi.org/10.1016/j.preteyeres.2015.07.001.
[48] D.P. Dowling, I.S. Miller, M. Ardhaoui, W.M. Gallagher, Effect of surface wettability and topography on the adhesion of osteosarcoma cells on plasma-modified polystyrene, J. Biomater. Appl. 26 (2011) 327–347, https://doi.org/10.1177/0885328210372148.
[49] H. Heslot, Artificial fibrous proteins: a review, Biochimie 80 (1998) 19–31, https://doi.org/10.1016/S0300-9084(98)80053-9.
[50] Q.N. Wei, A.M. Huang, L. Ma, Z. Huang, X. Huang, P.P. Qiang, Z.P. Gong, L. Zhang, Structure regulation of silk fibroin films for controlled drug release, J. Appl. Polym. Sci. 125 (2012), https://doi.org/10.1002/app.36901.
[51] S. Hofmann, C.T. Wong Po Foo, F. Rossetti, M. Textor, G. Vunjak-Novakovic, D.L. Kaplan, H.P. Merkle, L. Meinel, Silk fibroin as an organic polymer for controlled drug delivery, J. Control. Release 111 (2006) 219–227, https://doi.org/10.1016/j.jconrel.2005.12.009.
[52] Z. Pan, J. Ding, Poly(lactide-co-glycolide) porous scaffolds for tissue engineering and regenerative medicine, Interface Focus 2 (2012) 366–377, https://doi.org/10.1098/rsfs.2011.0123.
[53] M. Li, M. Ogiso, N. Minoura, Enzymatic degradation behavior of porous silk fibroin sheets, Biomaterials 24 (2003) 357–365, https://doi.org/10.1016/S0142-9612(02)00326-5.
[54] S. Verma, N. Kumar, Effect of biomimetic 3D environment of an injectable polymeric scaffold on MG-63 osteoblastic-cell response, Mater. Sci. Eng. C. 30 (2010) 1118–1128, https://doi.org/10.1016/j.msec.2010.06.005.
[55] J.W. Foster, R.M. Gouveia, C.J. Connon, Low-glucose enhances keratocyte-characteristic phenotype from corneal stromal cells in serum-free conditions, Sci. Rep. 5 (2015) 10839, , https://doi.org/10.1038/srep10839.
[56] D.H. Kim, D. Wirtz, Focal adhesion size uniquely predicts cell migration, FASEB J. 27 (2013) 1351–1361, https://doi.org/10.1096/fj.12-220160.
[57] D.L. Huang, N.A. Bax, C.D. Buckley, W.I. Weis, A.R. Dunn, Vinculin forms a directionally asymmetric catch bond with F-actin, Science (80-.) 357 (2017) 703–706, https://doi.org/10.1126/science.aan2556.
[58] L.E. Sidney, A. Hopkinson, Corneal keratocyte transition to mesenchymal stem cell phenotype and reversal using serum-free medium supplemented with fibroblast growth factor-2, transforming growth factor-β3 and retinoic acid, J. Tissue Eng. Regen. Med. 12 (2018) e203–e215, https://doi.org/10.1002/term.2316.
[59] W.C. Lee, J.P. Rubin, K.G. Marra, Regulation of alpha-smooth muscle actin protein expression in adipose-derived stem cells, Cells Tissues Organs 183 (2006) 80–86 (doi:95512 [pii]\n10.1159/000095512).
[60] G. Xu, M.L. Bochaton-Piallat, D. Andreutti, R.B. Low, G. Gabbiani, P. Neuville, Regulation of α-smooth muscle actin and CRBP-1 expression by retinoic acid and TGF-β in cultured fibroblasts, J. Cell. Physiol. 187 (2001) 315–325, https://doi.org/10.1002/jcp.1078.
[61] R. Mencucci, M. Marini, I. Paladini, E. Sarchielli, E. Sgambati, U. Menchini, G.B. Vannelli, Effects of riboflavin/UVA corneal cross-linking on keratocytes and collagen fibres in human cornea, Clin. Exp. Ophthalmol. 38 (2010) 49–56, https://doi.org/10.1111/j.1442-9071.2010.02207.x.
[62] Y. Zhang, A.H. Conrad, G.W. Conrad, Effects of ultraviolet-a and riboflavin on the interaction of collagen and proteoglycans during corneal cross-linking, J. Biol. Chem. 286 (2011) 13011–13022, https://doi.org/10.1074/jbc.M110.169813.
[63] K.M. Gronkiewicz, E.A. Giuliano, A. Sharma, R.R. Mohan, Effects of topical hyaluronic acid on corneal wound healing in dogs: a pilot study, Vet. Ophthalmol. 20 (2017) 123–130, https://doi.org/10.1111/vop.12379.
[64] L.T.Y. Ho, A.M. Harris, H. Tanioka, N. Yagi, S. Kinoshita, B. Caterson, A.J. Quantock, R.D. Young, K.M. Meek, A comparison of glycosaminoglycan distributions, keratan sulphate sulphation patterns and collagen fibril architecture from central to peripheral regions of the bovine cornea, Matrix Biol. 38 (2014) 59–68, https://doi.org/10.1016/j.matbio.2014.06.004.
[65] M. Gholipourmalekabadi, M. Mozafari, M. Gholipourmalekabadi, M. Nazm Bojnordi, M.B. Hashemi-Soteh, M. Salimi, N. Rezaei, M. Sameni, A. Samadikuchaksaraei, H. Ghasemi Hamidabadi, In vitro and in vivo evaluations of three-dimensional hydroxyapatite/silk fibroin nanocomposite scaffolds, Biotechnol. Appl. Biochem. 62 (2015) 441–450, https://doi.org/10.1002/bab.1285.
[66] L. Huang, J. Huang, H. Shao, X. Hu, C. Cao, S. Fan, L. Song, Y. Zhang, Silk scaffolds with gradient pore structure and improved cell infiltration performance, Mater. Sci. Eng. C. 94 (2019) 179–189, https://doi.org/10.1016/j.msec.2018.09.034.